CHALMERS
UNIVERSITY OF TECHNOLOGY

Optimal DC-Link Voltage Mapping for SiC-Based EV Drives: Considering the Impact of a Synchronous Boost Converter

Citation for the original published paper (version of record):
Amirpour, S., Thiringer, T., Soltanipour, S. et al (2025). Optimal DC-Link Voltage Mapping for SiC-Based EV Drives: Considering the Impact of a
Synchronous Boost Converter. IEEE Access, 13: 38239-3536.
http://dx.doi.org/10.1109/ACCESS.2025.3546025

(article starts on next page)

IEEE Access
Multidisciplinary ⋮ Rapid Review ⋮ Open Access Journal

Received 4 February 2025, accepted 20 February 2025, date of publication 26 February 2025, date of current version 6 March 2025.

Digital Object Identifier 10.1109/ACCESS.2025.3546025

RESEARCH ARTICLE

Optimal DC-Link Voltage Mapping for SiC-Based EV Drives: Considering the Impact of a Synchronous Boost Converter

SEPIDEH AMIRPOUR[1,2], TORBJÖRN THIRINGER[2,3], (Senior Member, IEEE), SIMA SOLTANIPOUR[2,3], (Member, IEEE), AND YU XU[1,2], (Member, IEEE)

[1]Zeekr Technology Europe, 41755 Gothenburg, Sweden
[2]Electrical Engineering Department, Chalmers University of Technology, 41296 Gothenburg, Sweden
[3]Volvo Car Corporation, Torslanda PVÖS22, 40531 Gothenburg, Sweden

Corresponding author: Sepideh Amirpour (sepideh.amirpour@zeekrtech.eu; sepideh.amirpour@chalmers.se)

This work was supported by Zeekr Technology Europe (ZEEKR) and Volvo Cars.

ABSTRACT This paper seeks to identify an optimal DC-link voltage across the complete range of drive operating conditions utilizing a loss minimization approach by integrating a DC-DC converter into the powertrain, thereby enhancing powertrain efficiency. This involves a comprehensive analysis of power losses in a connected silicon carbide (SiC)-based converter-inverter system, incorporating temperature variations, alongside a finite element method (FEM) analysis of losses in an Interior Permanent Magnet (IPM) synchronous machine, accounting for variable DC-link voltages. The results are then compared with those of traditional silicon-insulated-gate bipolar transistor (Si-IGBT) systems. The findings reveal that including a DC-DC converter into a powertrain, and adjusting the optimum DC-link voltages, is advantageous, particularly for low battery terminal voltages. Consequently, the powertrain system, incorporating a DC-DC boost converter, exhibits lower total loss values, with a difference of up to 5 kW loss difference for high-speed, low-torque regions compared to the case when not incorporating the DC-DC converter. Furthermore, applying the proposed optimal DC-link profile in the Worldwide harmonized Light vehicle Test Cycle (WLTC) leads to a reduction of up to 16% in accumulated energy losses in the SiC driveline compared to its IGBT counterpart. In addition, applying the optimal DC-link profile reduces energy losses by 58% in the SiC-based system and by 54% in the IGBT-based system, compared to operating with a fixed 300 V DC-bus voltage.

INDEX TERMS Electric vehicles, SiC-based motor drives, voltage-source inverters, dc-dc boost converter, permanent magnet synchronous machine, energy efficiency.

I. INTRODUCTION

Improving the efficiency of electric vehicle powertrains continues to be a key challenge. Recent advancements in Wide Band Gap silicon carbide (SiC) MOSFET technology have demonstrated significant potential for improving powertrain efficiency. This improvement is attributed to their faster switching dynamics, reduced on-state losses facilitated by their reverse conduction capability, and superior thermal performance compared to traditional silicon insulated gate bipolar transistors (Si IGBTs) [1], [2], [3]. However, fluctuations in the battery voltage present a notable challenge, as they can negatively impact energy efficiency and overall driving performance, as highlighted in [4], [5], [6], [7], and [8]. A viable solution to address this issue involves dynamically adjusting the DC-link voltage across various driving conditions to optimize powertrain efficiency. This approach employs a DC-DC boost converter connected to the battery, providing power to the pulse width modulation (PWM) traction inverter, rather than the conventional setup

The associate editor coordinating the review of this manuscript and approving it for publication was Xiaodong Liang.

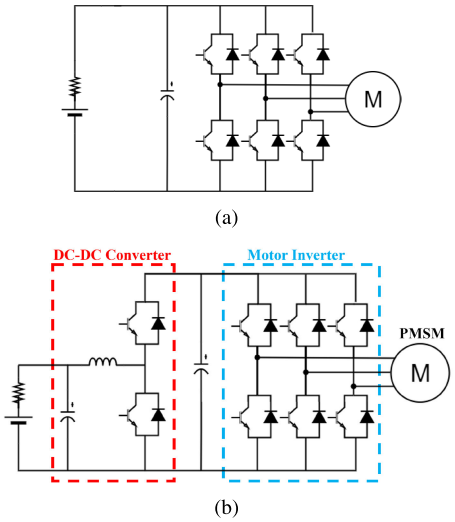

FIGURE 1. Voltage source inverter configuration.(a) Conventional EV powertrain. (b) Powertrain incorporating a synchronous DC-DC boost converter.

where the battery directly supplies the inverter. Both configurations, featuring IGBT switches, are illustrated in Figure 1.

At lower operating speeds, the required DC-link voltage is lower compared to the levels needed and desired at rated or high-speed operation. This is primarily due to the dependence of the back electromotive force (EMF) on motor speed. Consequently, a reduced DC-link voltage results in decreased switching losses within the inverter, thereby enhancing the overall efficiency of the drive system. In contrast, during rated or high-speed operation, including the field-weakening region, an increased DC-link voltage allows for a higher phase voltage. This adjustment can lower the motor current at higher rotational speeds, effectively reducing both the inverter's conduction losses and the copper losses in the machine. However, integrating a DC-DC converter into the powertrain system adds additional passive components, increases system complexity, raises costs, and results in reduced reliability, as highlighted in the literatures [9], [10], [11], and [12]. In [12] despite showing substantial energy savings achieved with a DC-DC converter and optimized battery voltage compared to conventional systems, it is concluded that, the advantage of a boost converter grows if as more operating points shift to lower speeds. Various studies have explored methods to improve powertrain efficiency by optimizing the DC-link voltage through the use of a DC-DC converter [13], [14], [15], [16], [17], [18], [19]. [13] focuses on replacing flux weakening with a DC voltage boost, analyzing motor efficiency gains from voltage boosting but without accounting for additional power electronics losses or high-power applications. In [14] an experimental setup is provided for an integrated power unit consisting of an inverter to feed an interior permanent magnet synchronous machine (IPMSM) and a DC-DC converter; the paper addresses differences in control strategies and identifies operating regions with improved efficiency; however, clear and detailed loss calculations for both the machine and converters (inverter and DC/DC converter) were not conducted in this article and lacks a detailed finite element (FEM) machine loss breakdown. References [15] and [16] presents an optimum DC bus voltage analysis that mitigates parameter errors and machine spatial harmonic effects and [17] analyzes the added value of dynamic DC-link voltage adaptation for the thermal management of traction drives. While interesting, the analyses are limited to a traditional IGBT-based drive system and do not include a DC-DC converter or its associated losses. Reference [18] develops a variable DC link scheme for a closed-loop induction motor drive, using a front-end DC-DC buck converter between the fixed DC bus and IGBT-based inverter. However, only the power electronics losses are considered to determine the optimal DC link voltage, excluding machine losses. Reference [19] compares a SiC MOSFET-based adjustable DC-link voltage powertrain with its IGBT-based counterpart, including a DC-DC converter. However, the impact of temperature variations on powertrain losses and the converter's inductance losses are not explored. Finally, the authors' previous work, as presented in [20], accounts for temperature variations in the power electronics losses. However, inductor losses were not considered in that study, nor was the analysis extended to include the IGBT counterparts.

To sum up, despite valuable research in the above articles, a comprehensive loss analysis remains lacking. In particular, losses associated with the DC-DC converter, including switches and inductance losses, should not be underestimated. Additionally, the effect of temperature variations on power electronics losses and machine performance have rarely been evaluated. Consequently, to the best of the authors' understanding, the decision to include a DC-DC converter is not clearly justified.

In light of this, building on the authors' previous research presented in [20], this study seeks to bridge the above-mentioned gaps by producing comprehensive powertrain loss maps, which serves as a key metric for accurately identifying the optimal DC-link voltage across the entire drive range. In this context, the key contributions of this work are summarized as follows:

- Performing a comprehensive system-level loss analysis that integrates; FEM-based loss modeling for the permanent magnet synchronous machine (PMSM) under variable DC-link voltages. Power electronics losses from the linked converter-inverter system, while incorporating junction temperature feedback and blanking time effects into the analysis to enhance accuracy.
- Designing and integrating an inductor for the DC-DC converter, optimized for full-load conditions, with its associated losses incorporated into the total powertrain loss evaluation.
- Leveraging the generated full loss maps to determine the optimal DC-link voltage across the entire drive operating range, using a loss-minimization approach over a wide range of rotor speeds and torque conditions.

The comprehensive calculation of total system-level losses, along with the determination of optimal DC-link voltage profiles, were then performed for the IGBT-based system, incorporating the effects of inductance losses and results were compared to those of the SiC-based system. In addition, an energy loss and drive cycle analysis was conducted for both SiC and IGBT powertrains, allowing for a comparative evaluation.

Therefore, the proposed detailed system-level loss analysis offers a clearer understanding of the benefits of adjustable DC-link voltage for both SiC- and IGBT-based powertrains with DC-DC converters. Additionally, it achieves greater accuracy in total loss mapping, enabling the identification of the optimal DC-bus voltages across the entire drive range.

The remainder of this paper is organized as follows: Section II outlines the study's case setup, providing a detailed explanation of the simulation configurations, co-simulation setups, and drive parameters used in this work. Section III describes the analytical power loss models for the three-phase inverter and DC-DC converter, incorporating numerical modeling of temperature feedback, blanking time, and MOSFET reverse conduction. This section also discusses the utilized electric machine and the derivation of its associated losses. Section IV presents the complete analysis, including the mapping of the optimal DC-link bus voltage across the entire torque–speed region of the drive system, using a loss minimization approach for both SiC- and IGBT-based powertrains. Finally, Section V summarizes the study's conclusions.

II. CASE SETUP

The aim of this case setup is to determine the optimal DC-link voltage for the full range of drive operating conditions by incorporating a DC-DC converter into the powertrain. To reach this aim, a 2-D FEM model of an IPMSM—created in Maxwell—was employed, as illustrated in Figure 2. The stator features 48 slots, and to enhance computational efficiency, the model was reduced to one-eighth of its original size by leveraging the symmetry of eight identical poles.

The FEM analysis was performed by applying current excitation to the coils and assigning appropriate boundary conditions. A transient simulation was then conducted under various operating conditions. Next, using the d- and q-axis reference currents derived from the FEM results, the maximum torque per ampere (MTPA) and maximum torque per volt (MTPV) control strategies [21], [22] were implemented via a co-simulation framework between Ansys Electronic Desktop and MATLAB, enabling the mapping of key operating points across the machine's torque—speed range.

A three-phase voltage source inverter (VSI) was numerically implemented, and then connected to a DC-DC boost converter for the purpose of this case study, as shown in Figure 1(b). The converter-inverter circuit incorporates power modules, including a half-bridge SiC module, CAB450M12XM3 [23], and a Si IGBT module, FZ600R12KE3 [34] for the comparisons. In the SiC-based converter-inverter, four SiC half-bridge modules (one for the converter and three for the inverter) were used, with one MOSFET for each switch position. For the IGBT-based inverter, six IGBT modules, one in each switch position, and two modules for the converter, were employed to meet the respective design specifications in each analysis. The parameters for the drive system used in this case study are provided in Table 1.

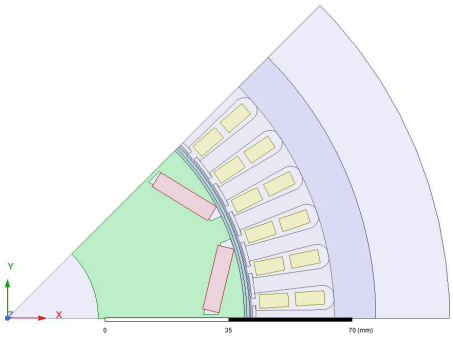

FIGURE 2. The 2-D IPMSM model in ANSYS maxwell.

TABLE 1. PMSM drive system parameters.

Parameter	Value	Unit
Number of slots	48	—
Number of poles	4	—
Peak current	400	A
Peak torque	333.3	Nm
Maximum rotor speed	11000	rpm
Switching frequency	10	kHz
Blanking time	0.5	µs

It is worth noting that an inductor was designed for the DC-DC converter. The theory and design steps will be presented in the respective section.

Subsequently, the mapped operating points derived from the above-mentioned co-simulation were then utilized in the inverter as well as the converter-inverter loss calculation model, incorporating the junction temperature feedback of the semiconductor devices. Figure 3 illustrates an overview of the analysis.

III. POWERTRAIN LOSS MODELING

This section focuses on the development of analytical models for powertrain component losses. These models provide the basis for the numerical adjustment of the DC-link voltage across the full drive region, as discussed in subsequent sections.

A. THREE-PHASE INVERTER COUPLED WITH DC-DC CONVERTER

As previously discussed, the latest advancements in commercial Wide Bandgap (WBG) SiC MOSFETs offer a promising alternative to traditional Si IGBTs for electrified vehicle applications. Their advantages stem from significantly lower

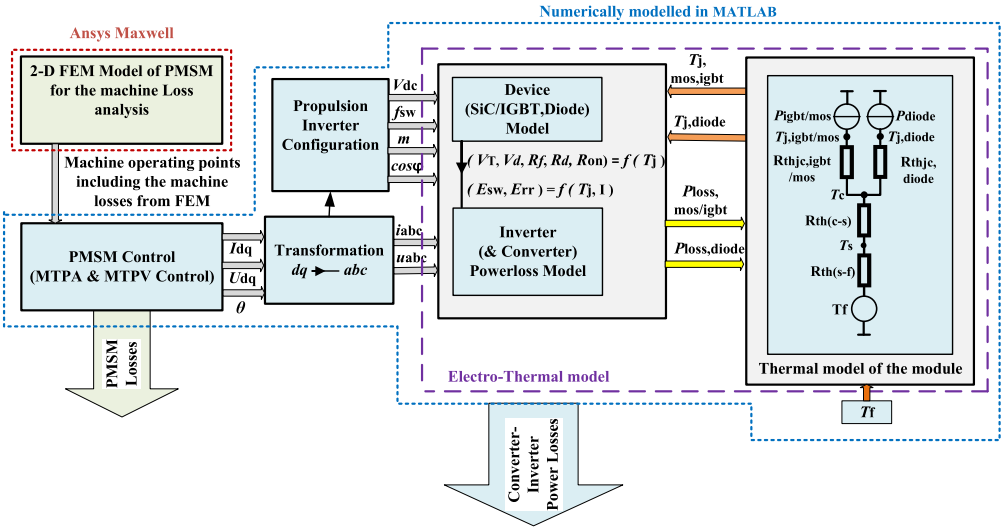

FIGURE 3. Analysis overview.

switching losses due to faster transition times and enhanced thermal performance, making them a preferred choice over Si IGBTs. Additionally, the reverse conduction capability of MOSFETs contributes to reduced conduction losses. To effectively leverage the energy-saving potential of the variable DC-link voltage strategy, a third-generation half-bridge SiC module, CAB450M12XM3 [23], has been utilized for the development of converter-inverter loss models. The circuit configuration is similar to the one depicted in Figure 1, where a synchronous SiC-based boost converter connected to the inverter is used to map the DC-link voltage across the full operating range.

1) CONDUCTION LOSSES

The conduction losses for a three-phase voltage source inverter and a DC-DC converter are computed numerically using MATLAB. This numerical implementation is based on an analytical method for estimating conduction losses in SiC MOSFETs, as described in [24] and [25]. Using this method, the average conduction losses of the MOSFETs over one fundamental period of the phase current can be determined as

$$P_{\text{cond,MOS}} = \frac{1}{2\pi}\int_0^{2\pi} R_{\text{on}} {I_{\text{M}}}^2(\alpha)\tau(\alpha)d\alpha \tag{1}$$

where R_{on} is the MOSFET on-state resistance, I_{M} is the MOSFET current, $\alpha = 2\pi ft$ where f is the fundamental frequency and τ is the duty cycle which can be expressed as a function of α as

$$\tau(\alpha) = \frac{1}{2}(1 + m\sin\alpha) \tag{2}$$

where m is the modulation index [26]. Likewise, the diode conduction losses can be derived as

$$P_{\text{cond,D}} = \frac{1}{2\pi}\int_0^{2\pi} (R_{\text{d}} {I_{\text{D}}}^2(\alpha) + V_{\text{d}} I_{\text{D}}(\alpha))\tau(\alpha)d\alpha \tag{3}$$

where the voltage drop, V_{d}, and the on-state resistance, R_{d}, can be obtained from the datasheet information of the forward characteristics of the diode. Finally, I_{D} is the diode current.

It is important to note that the current flowing through the DC-DC converter is assumed to remain at a constant amplitude during a single pulse period, with fluctuations smoothed by the inductance. Under this assumption, the duty cycle D of the boost converter can be calculated as

$$D = 1 - \frac{V_{\text{batt}}}{V_{\text{dc}}} \tag{4}$$

where V_{batt} is the battery terminal voltage and V_{dc} is the DC-link voltage.

- **MOSFETs Reverse Conduction:**
  During reverse conduction, the MOSFETs and diodes within a phase leg of the SiC inverter share the reverse current, leading to a substantial reduction in the diodes' overall conduction losses. The current through the MOSFET and diode can be determined as

$$I_{\text{M}} = \frac{R_{\text{d}} I_{\text{p}}\sin(\alpha - \varphi) - V_{\text{d}}}{R_{\text{d}} + R_{\text{on}}} \tag{5}$$

$$I_{\text{D}} = \frac{R_{\text{on}} I_{\text{p}}\sin(\alpha - \varphi) + V_{\text{d}}}{R_{\text{d}} + R_{\text{on}}} \tag{6}$$

  where φ is the angle of displacement power factor and I_{p} is the peak phase current [24], [25]. Therefore, to accurately determine losses in SiC-based devices, this capability of the MOSFETs is numerically modeled in MATLAB and incorporated into the inverter loss simulations.
- **Blanking Time:**
  The effect of blanking time on the calculation of conduction power losses can be accounted for by introducing an equivalent duty cycle. This equivalent duty cycle is then applied in the previously mentioned

conduction loss equations.

$$\tau_{\text{eq}}(\alpha) = \tau(\alpha) - t_{\text{blanking}} f_{\text{sw}} = \frac{1}{2}(1 - 2t_{\text{blanking}} f_{\text{sw}} + m \sin\alpha) \quad (7)$$

where f_{sw} is the switching frequency [24], [25].

Previous work by the authors has provided a detailed examination of the influence of MOSFET reverse conduction and blanking time on the power losses of the investigated SiC module [24], [27].

2) SWITCHING LOSSES

Switching losses occur during each turn-on and turn-off event in both the switch and its anti-parallel or body diode. These losses can be analytically determined for a MOSFET and a diode using the following expression,

$$P_{\text{sw,MOSFET,IGBT,Diode}} = f_{\text{sw}} \cdot E_{\text{sw}(\text{I}_{\text{nom}}, \text{V}_{\text{nom}})} \cdot \left(\frac{1}{\pi} \frac{I_{\text{p}}}{I_{\text{nom}}}\right)^{k_{\text{i}}} \cdot \left(\frac{V_{\text{dc}}}{V_{\text{nom}}}\right)^{k_{\text{v}}} \quad (8)$$

where E_{sw} is switching energy loss, I_{p} is the peak phase current, I_{nom} and V_{nom} are nominal current and voltage values and k_{i}, k_{v} are current and voltage dependency exponents, respectively [28]. (According to [28], the typical exponent values for IGBTs are selected as ($k_{\text{iD}} = 1$; $k_{\text{vD}} = 0.6$; $k_{\text{iIGBT}} = 1$; $k_{\text{vIGBT}} = 1.35$). The exponent values are chosen equally for MOSFET modules as ($k_{\text{iD}} = 1$; $k_{\text{vD}} = 1$; $k_{\text{iMOSFET}} = 1$; $k_{\text{vMOSFET}} = 1$). I_{nom} and V_{nom} represent the nominal (reference) currents and voltages, as specified in the modules' datasheets.) In this study's numerical implementation, the switching loss is computed for each switch-on and switch-off event of the device as

$$P_{\text{sw}} = \frac{\sum E_{\text{sw}}}{t} \quad (9)$$

where t is the fundamental period of time.

3) THERMAL MODELING

Since certain parameters in power modules, including on-state resistances, forward voltage drops, and switching and reverse recovery energies, are temperature-dependent, the inverter power losses are calculated using a thermal network, as shown in Figure 4, configured for the modules. T_{j}, represents the junction temperatures of MOSFETs and diodes, T_{c} is the case/baseplate temperature, T_{s} and T_{f} represent the heatsink and fluid temperatures, respectively. The thermal resistances from the junction to case, case to sink, and sink to fluid, represented by $R_{th,jc}$, $R_{th,cs}$, and $R_{th,sf}$, respectively, can be expressed by,

$$R_{th,jc} = \frac{T_j - T_c}{P_{loss}} \quad (10)$$

$$R_{th,cs} = \frac{T_c - T_s}{P_{loss}} \quad (11)$$

$$R_{th,sf} = \frac{T_s - T_f}{P_{loss}} \quad (12)$$

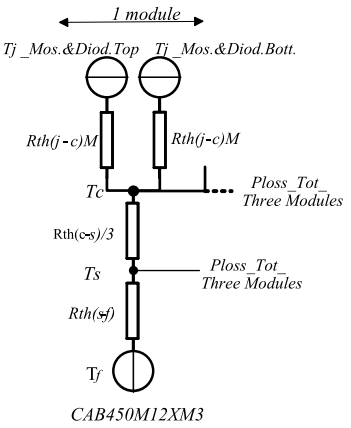

FIGURE 4. Thermal calculation model for the used SiC module in the converter-inverter system.

Then, the junction temperature can be modeled as

$$T_j = T_f + (R_{th,jc} + R_{th,cs} + R_{th,sf}) P_{loss} \quad (13)$$

where P_{loss} represents the associated losses of the module's devices in each thermal stack-up layer, as illustrated in the figure.

It is noteworthy that the fluid temperature and flow rate are set at 65 $^{\circ}C$ and 10 L/min, respectively. The thermal resistance data used in the thermal network are obtained from the module's datasheet and the heatsink's datasheet [29], [30]. Note that, the CAB450 module features the latest 3rd-generation MOSFET dies with an integrated body diode, eliminating the need for an antiparallel diode.

The total losses are determined using an iterative approach that accounts for temperature. In this method, the devices' static and dynamic parameters (V_{d}, R_{d}, R_{on}, E_{sw} and E_{rr}) are numerically interpolated based on a given junction temperature. The losses and temperatures are then recalculated iteratively until convergence is reached [24]. The current dependency of the devices' switching energies is also modeled as a function of both current and junction temperature. Figure 5 shows the flowchart for estimating junction temperature of the module's devices in steady-state using the thermal calculation model given in Figure 4, and the above-mentioned equations.

B. ELECTRIC MACHINE

This research employs a PMSM model, with the operating points systematically mapped according to the primary drive parameters listed in Table 1. A field-oriented control (FOC)-based PMSM drive system, incorporating MTPA and MTPV control strategies [21], [22], was implemented through a co-simulation framework using Ansys Electronic Desktop and MATLAB. Consequently, loss calculations were performed across the operating range for the DC-link voltage, spanning from 220 V to 450 V.

The MTPA control strategy, commonly utilized for PMSMs, is optimized to deliver specific torque at a given speed while minimizing current consumption, thereby

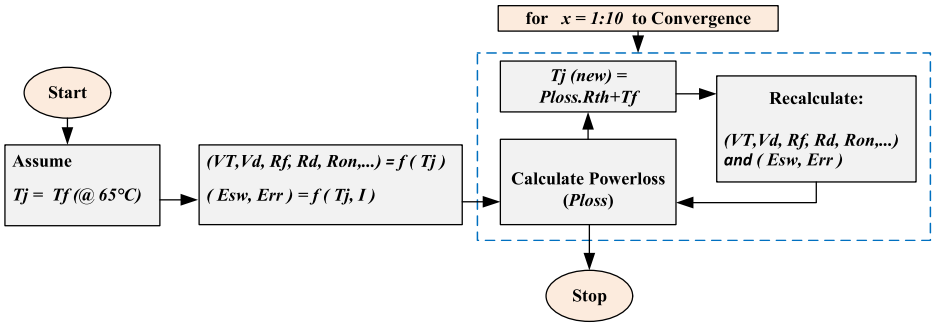

FIGURE 5. Flow chart for estimating the junction temperature in steady-state.

reducing copper losses in the machine. However, this strategy relies on the available DC voltage. The corresponding speed, known as the base speed, denotes the maximum speed at which the motor can operate under the MTPA strategy without encountering voltage limitations.

Once the motor exceeds the base speed, the field-weakening strategy is employed by introducing a negative I_d current (in dq-axis plane) to decrease the effect of the magnet flux. This approach allows the motor to operate at higher speeds within the given voltage constraints. However, it leads to increased motor losses and a reduced maximum torque output, as the motor now operates outside its optimal MTPA range.

An increase in the supplied DC voltage expands the voltage ellipse in the dq-axis plane, thereby raising the base speed. This enlargement allows the MTPA region to cover a broader speed range. Within the constraints of the voltage limit and the MTPA region, variations in DC voltage have little effect on the I_d and I_q currents. Consequently, copper losses remain unchanged despite fluctuations in the supplied DC voltage [19], [21], [22].

To address the non-linearity inherent in PMSMs and accurately estimate losses, finite element analysis (FEA) simulations are conducted using Ansys Maxwell in conjunction with MATLAB. These simulations calculate key electromagnetic losses, including copper losses and core losses which encompass hysteresis and eddy current losses.

The d- and q-axis reference currents for the MTPA/MTPV control strategy are derived using the FEA analysis. With these control algorithms, a comprehensive mapping of key operating points within the machine's torque-speed region has been performed. These mapped operating points are then utilized in the converter-inverter loss calculation model outlined in the previous section. The calculations cover a range of supplied DC voltages, from 220 V to 450 V, representing the lower and upper boundaries of the DC-link voltage, with their implications discussed in subsequent sections.

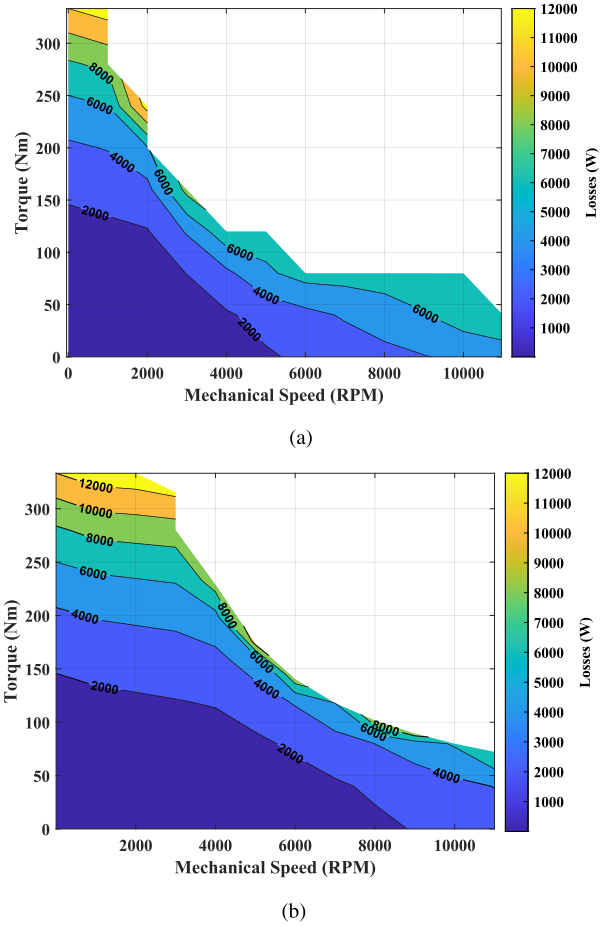

FIGURE 6. EV powertrain system total losses including machine and inverter.(a) at 220 V dc-bus voltage. (b) at 450 V dc-bus voltage.

IV. RESULTS ANALYSIS

A. SiC-BASED ELECTRIC POWERTRAIN LOSS ANALYSIS UNDER VARIABLE DC-LINK VOLTAGE

A detailed powertrain model, integrating advanced power electronics loss models and control algorithms, has been developed within the MATLAB and Ansys Maxwell environment. This model is used to validate the proposed topology, with a particular emphasis on finding the optimal DC-link voltage across the entire drive region.

The initial phase of the analysis focused on calculating the total losses, encompassing both the machine and inverter components, at the DC-link voltage boundaries of 220 V and 450 V. The results indicated that the machine exhibited greater differences in losses between the two DC-link voltage levels compared to the inverter, which showed only minor

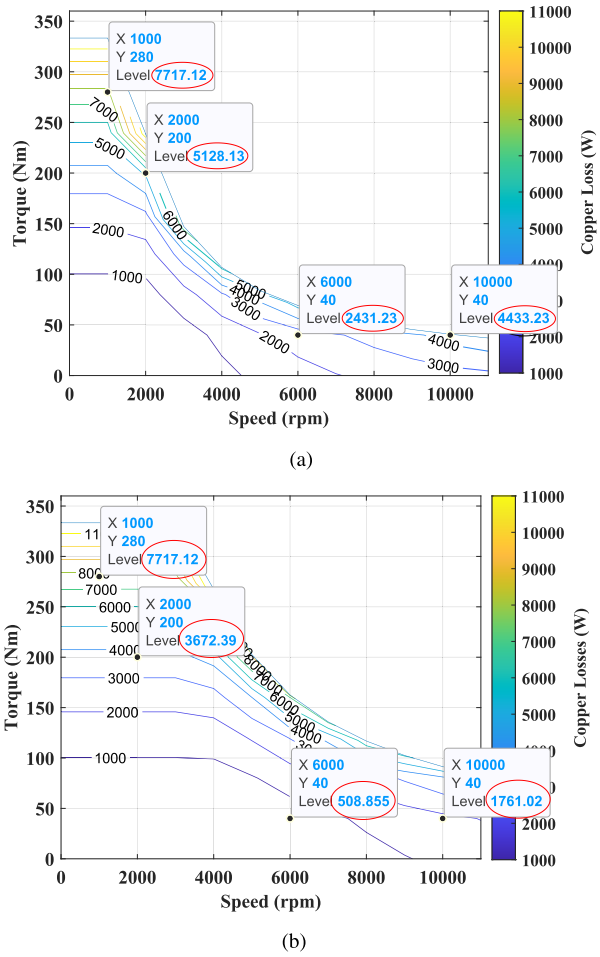

FIGURE 7. Calculated copper losses across the entire drive region with indicators for four operating points.(a) Copper losses at 220V DC-link. (b) Copper losses at 450V DC-link.

variations in losses. However, both the machine and inverter experienced lower losses at a DC-link voltage of 450V, particularly in the field-weakening region. Accordingly, the total system losses (machine + inverter) for the two DC-link voltages, illustrated in Figure 6, reveals that the field-weakening region experiences lower losses with a 450V DC-link compared to 220V. This is because a higher DC-link voltage enables the inverter to generate higher output voltages, facilitating effective field weakening at elevated speeds. Conversely, if the DC-link voltage is too low, the inverter cannot provide sufficient voltage to weaken the field, reducing the motor efficiency in high-speed operation. Furthermore, a lower DC-link voltage requires a higher current to deliver the same power, which results in higher resistive losses. This, in turn, reduces the overall efficiency of the motor and the powertrain.

Subsequently, a detailed loss analysis of the machine indicated that copper losses account for a substantial portion of the total machine losses, particularly when compared to other calculated machine losses, in relation to the DC-link voltage. This observation is illustrated in Figure 7, which highlights four distinct operating points detailed in Table 2,

TABLE 2. Four selected operating points on the drive region.

OP. 1	OP. 2	OP. 3	OP. 4
1000 rpm 280 Nm	2000 rpm 200 Nm	6000 rpm 40 Nm	10000 rpm 40 Nm

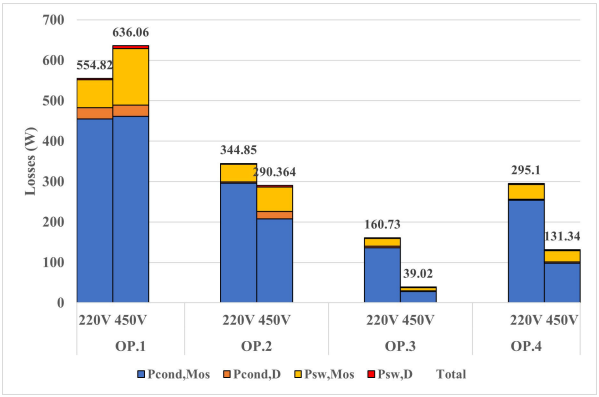

FIGURE 8. Conduction and switching losses of MOSFETs and diodes at four selected operating points, compared between DC-link voltages of 220V and 450V.

encompassing both the low-speed, high-torque region and the high-speed, low-torque region.

As shown, copper losses remain unaffected by the DC-link voltage at the first marked operating point in the low-speed, high-torque region (below base speed). However, as the speed increases—particularly in the mid-speed, low-torque region (the third marked operating point, OP.3)—the machine experiences notably higher copper losses, five times higher, with a low DC-link voltage compared to the higher DC-link one.

A parallel analysis of inverter losses was performed for the four investigated operating points, with the results presented in Figure 8.

From the figure, it is evident that MOSFET conduction losses represent a substantial share of the total inverter losses. Similar to the machine's copper losses, variations in the DC-link voltage reveal that the third operating point, situated in the high-speed, low-torque region, leads to greater losses with a lower DC-bus voltage. Additionally, MOSFET switching losses, which are a secondary contributor to inverter losses, exhibit a similar dependency on lower DC-link voltages.

The subsequent analysis examined the junction temperature variations of the inverter semiconductors at the two DC-link voltage levels, 220 V and 450 V. Notable temperature increases were observed, with junction temperatures rising by up to 20 °C in the mid-speed region and up to 14 °C in the high-speed, low-torque region when the lower DC-link voltage was applied. These findings are depicted in Figure 9.

In the next phase, the battery's open circuit voltage and internal resistance, both influenced by the state of charge (SoC), were incorporated into the loss calculations for the DC-DC boost converter. Two scenarios were analyzed to account for variations in the battery terminal voltage. The

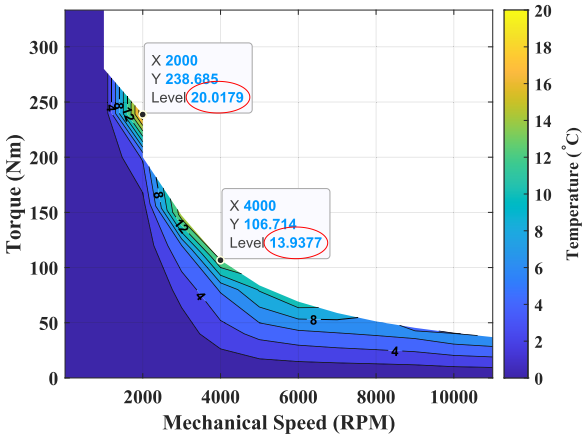

FIGURE 9. Observed junction temperature difference in MOSFETs between DC-link voltages of 220V and 450V.

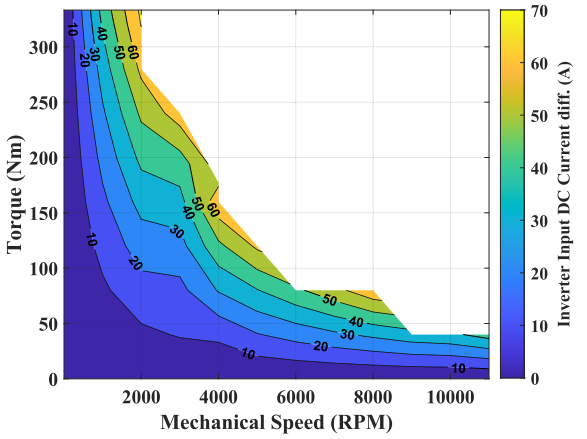

FIGURE 11. Difference in inverter input DC current between 330V and 450V DC-link voltages.

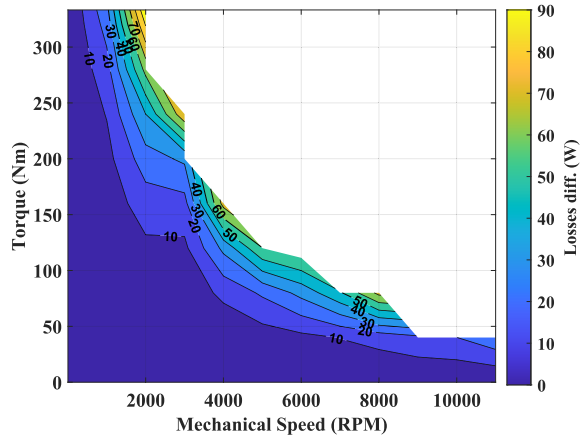

FIGURE 10. Loss difference in DC-DC converter when boosting to 330 V vs 450 V from 300 V battery voltage.

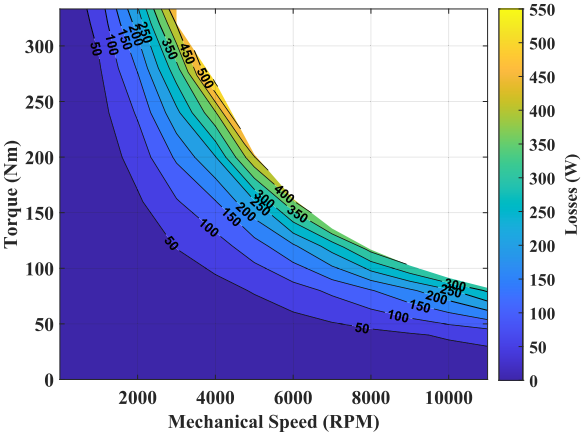

FIGURE 12. Power electronics losses in the SiC-based converter boosted from 300 V to 450 V DC-bus.

worst-case scenario assumes that the terminal voltage drops to 220 V DC, either temporarily for stabilization or under low SoC conditions. The second scenario considers the voltage stabilizing within the range of 300 V. For both cases, converter power losses were evaluated for boosting to 330 V, 400 V, and 450 V, aiming to identify the conditions that result in the lowest losses.

In both scenarios, with battery terminal voltages at 220 V and 300 V, the converter exhibited higher loss values when boosting to the lower DC-link voltage of 330 V compared to 450 V. Figure 10 illustrates the difference in losses between boosting from 300 V to 330 V and boosting from 300 V to 450 V in the second scenario. As shown, boosting to the lower value of 330 V results in increased losses relative to 450 V DC. The discrepancy reaches up to 100 W in high-torque, low-speed regions and up to 70 W in the field-weakening region, specifically within the speed range of 6000 RPM to 9000 RPM.

This is attributed to the increased inverter input DC current, which flows directly through the upper-side MOSFET of the boost converter. When comparing the lower DC-link voltage of 330 V to 450 V, this current difference reaches up to 70 A, as shown in Figure 11. As a result, the MOSFET incurs higher losses, primarily in conduction losses, leading to an overall increase in total losses for the DC-DC converter when boosting to the lower DC-link voltage of 330 V.

The results led to the next step; evaluating the potential benefits of integrating a DC-DC converter into the EV powertrain. Figure 12 illustrates the power electronics losses in a SiC-based DC-DC converter when boosted from a 300 V to a 450 V DC-link. To achieve an accurate approximation of the losses introduced by the DC-DC converter– including semiconductor power losses– an efficient inductor for a full load condition (peak DC current) was designed, and its core and copper losses were assessed and included in the analysis as follows.

- **Inductor Core Selection:**
  Selecting an optimal core for a given design specification, particularly in high-power applications, can be challenging due to many factors involved in the design. For instance, considering the required inductance value at full-load DC current, a Toroid powder core with

TABLE 3. Selected inductance core parameters.

Parameter	Value	Unit
Battery terminal voltage	300	Vdc
DC-link voltage	450	Vdc
Peak DC current	290	A
Switching frequency	10	kHz
Inductance value	115	uH
Number of stacked cores	2	—
Number of wire strands	5	—
Wire size	6	AWG
Number of turns	51	—

XFlux material from MAGNETICS, model 0078163A7 [31], was selected as the most efficient choice. Powder cores are distributed air-gap cores known for their high resistivity, minimal hysteresis and eddy current losses, and excellent inductance stability under both DC and AC conditions [32]. Table 3 gives the required inductor design values and selected core parameters. To begin with, the required inductor value was calculated based on the peak required DC current in the converter and a peak-to-peak current ripple of 20 % of the DC current,

$$L = \frac{V_{\text{in}} DT}{2\Delta I_{\text{L,peak}}} \tag{14}$$

where V_{in} is the battery terminal voltage, D is the duty cycle of the boost converter, T is the period time and $\Delta I_{\text{L,peak}}$ is the peak inductor ripple current.
Following, using the inductance factor $A_{\text{l}}(nH/T^2)$ from the core datasheet and the required number of core stack, the approximate number of turns can be calculated as,

$$N = \sqrt{\frac{L}{A_{\text{l}}}} \tag{15}$$

To meet the required inductance value, the number of turns can be adjusted by calculating the magnetizing field H Oersteds (Oe) as follows, considering the initial permeability at the calculated H bias level [32], and iterating the calculations if necessary.

$$H = \frac{4\pi NI}{l_{\text{e}}} \tag{16}$$

where I is the DC current and l_{e} is the magnetic path length.

- **Core and Copper loss Analysis:**
Core loss arises from changes in the magnetic flux field within a material. The core loss density, $P_{\text{L}}(mW/cm^3)$, is generally a function of the peak AC flux swing, B_{peak} in $Tesla(T)$, and the operating switching frequency. This loss can typically be approximated using manufacturer-provided core loss charts or by applying the Steinmetz loss equation [33], which provides a curve-fit model for estimating losses under given flux and frequency conditions,

$$P_{\text{L}} = kB_{\text{peak}}{}^{\alpha} f^{\beta} \tag{17}$$

$$B_{\text{peak}} = \frac{\Delta B}{2} \tag{18}$$

where k, α and β can be determined from curve fitting. Worth mentioning is that, since flux density B is a nonlinear function of magnetic field (H), B_{peak} can be calculated by first finding the maximum and minimum values of H. By evaluating H at these extremes, the corresponding B values can then be determined, allowing for the accurate calculation of B_{peak}. Accordingly, considering the number of stacks in the core valume, core loss has been calculated as,

$$P_{\text{fe}} = P_{\text{L}} l_{\text{e}} A_{\text{e}} = P_{\text{L}} V_{\text{e}} \tag{19}$$

where A_{e} and V_{e} are the effective cross-sectional area and volume of the core, respectively, both of which are provided in the core's datasheet.
Finally, the DC copper loss of the inductor or wire loss was calculated directly as,

$$P_{\text{cu}} = Resistance.I^2 \tag{20}$$

where *Resistance* is the product of the datasheet parameters: the mean length of turn, the number of turns, and the resistance per unit length for the selected wire gauge.
Consequently, the above-mentioned losses were evaluated for the designed inductance of the boost converter across the full range of drive operating points, as shown in Figure 13. As illustrated, the largest portion of losses arises from copper losses, which have already been reduced by using multiple strands.

Subsequently, the total system losses were analyzed for both scenarios across all drive operating points, both with and without the integration of the DC-DC converter.

It was observed that the powertrain system incorporating a DC-DC boost converter in both scenarios—boosting from a 220 V battery terminal to a 450 V DC-link voltage and from 300 V to 450 V—demonstrates lower total loss values, particularly in high-speed, low-torque regions. This contrasts with the scenario where the DC-DC converter is excluded.

Figure 14 illustrates the system losses for the second scenario, which involves boosting from a 300 V battery terminal, both with and without the integration of a DC-DC converter. Initially, the system losses, including those of the machine and the SiC-based inverter, were calculated for a 300 V battery terminal, see Figure 14 (a). Subsequently, a SiC-based DC-DC boost converter was added to the system, and the total losses were recalculated for a boosted 450 V DC-link voltage, as shown in Figure 14 (b). While the inclusion of the DC-DC converter increases the total system losses, particularly in the low-speed, high-torque region, significant improvements are observed in the field-weakening region, as anticipated. As illustrated in Figure 14 (c), the loss difference between the two configurations can reach up to 5 kW. As expected, in the low-speed region below the base speed, the loss difference ranges from zero to negative values (see the contour bar), indicating that, under the design specifications of this study, incorporating the DC-DC

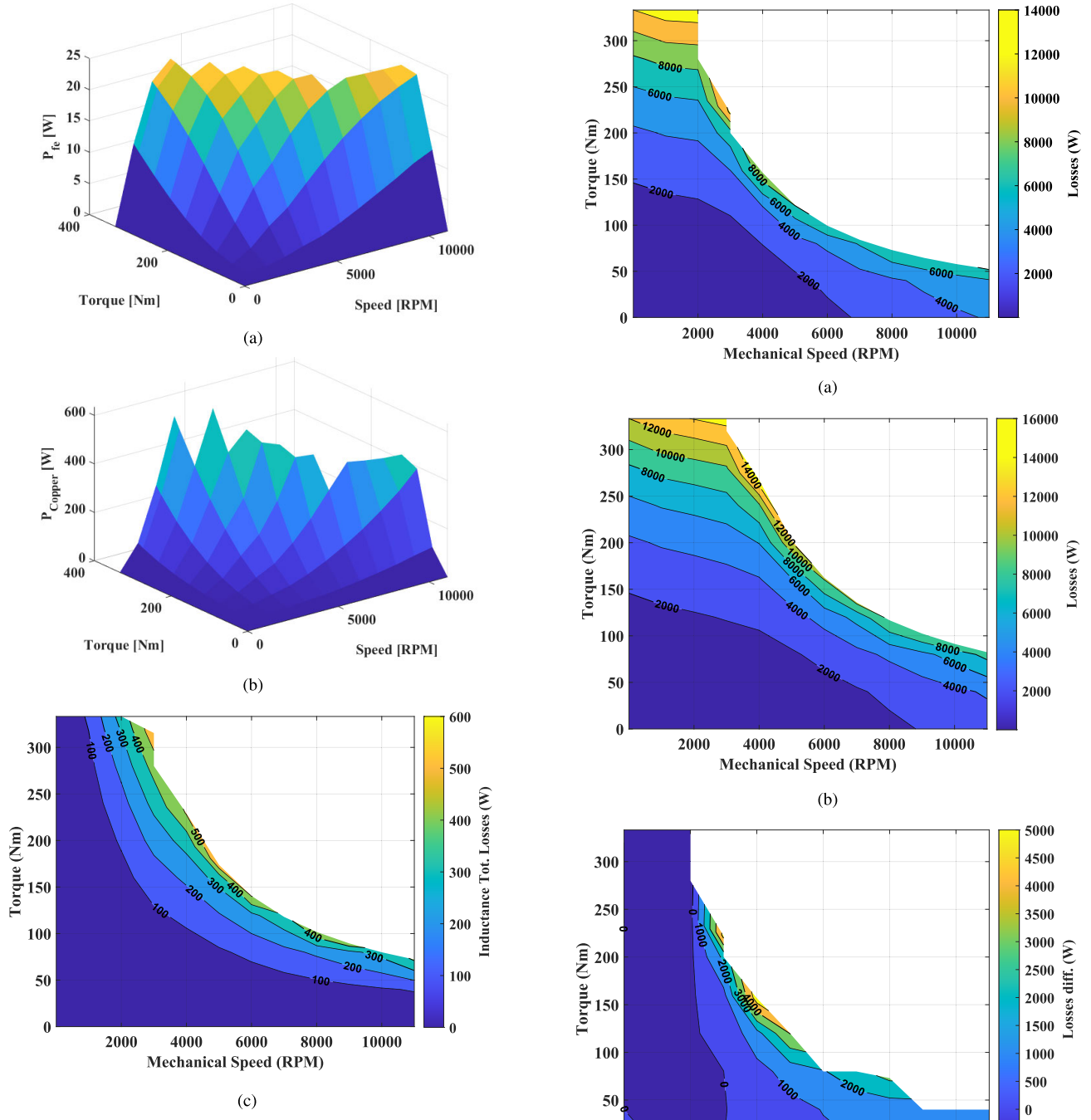

FIGURE 13. Inductance losses of the DC-DC converter over the entire drive operating points.(a) Core losses. (b) DC copper losses. (c) Total losses.

converter to boost to 450 V does not enhance the drive system efficiency in this region.

This observation can be explained by considering the dependence of inverter switching losses on the DC-link voltage, especially in the low-speed regions. Higher DC-link voltages lead to increased losses in this region. However, the use of SiC MOSFETs, which have much lower switching energy loss compared to IGBTs, contributes to this minimal loss difference in this region. If IGBT-based inverters were

FIGURE 14. Total losses in the SiC-based system and the loss difference with and without the DC-DC converter. (a) System losses including inverter and machine at 300V DC-bus. (b) System losses including inverter, machine, and DC-DC boost from 300V battery terminal to 450V DC bus. (c) Differences in system losses with and without the DC-DC converter; figure(a)-figure(b).

used instead, the difference in losses in this region (i.e., losses for 300 V DC-bus minus losses for 450 V DC-bus) would likely be greater, as will be discussed in a later section.

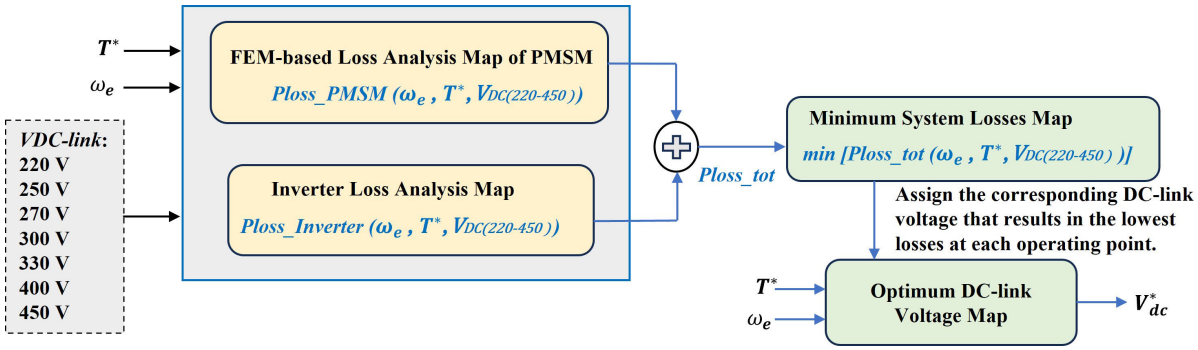

FIGURE 15. Steps to identify the optimal DC-link voltage over the entire range of the drive system.

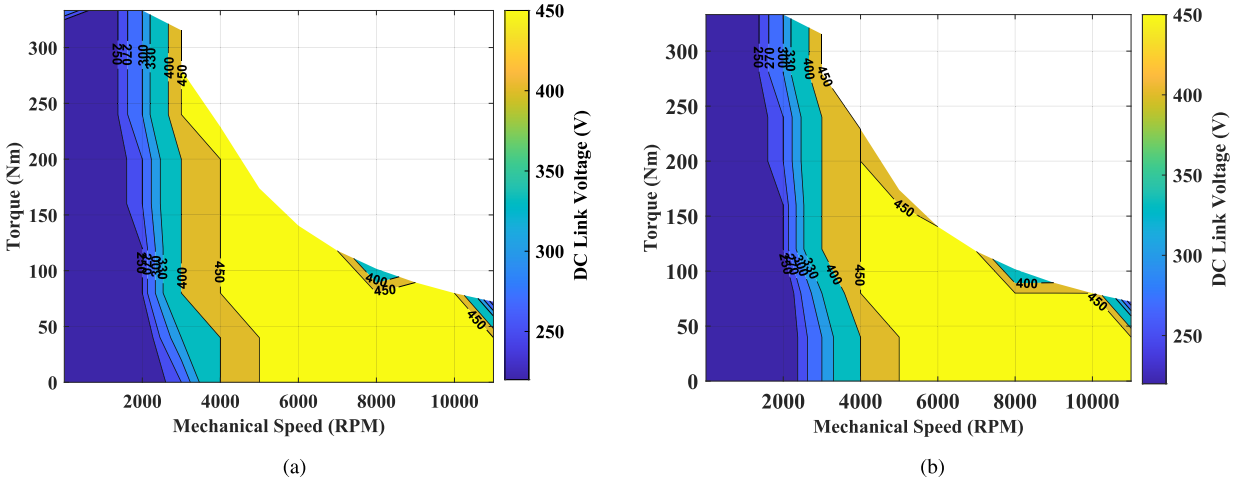

FIGURE 16. Optimum dc-bus voltages are assigned across the entire drive operating region.(a) Lowest loss Vdc-based regions for the machine. (b) Lowest loss Vdc-based regions for the inverter.

B. OPTIMAL DC-LINK VOLTAGE SCHEME: OVERALL SIC POWERTRAIN SYSTEM

Following the process illustrated in Figure 15, a comprehensive system-level loss analysis was performed across a discrete set of DC-link voltages (220–450 V) and torque–speed operating points. This approach employs an exhaustive (brute-force) search to determine which voltage minimizes total system losses at each point, effectively serving as an offline optimization method. The procedure can be summarized as follows:

- **Specifying all candidates:** Generate a set of possible DC-link voltages (e.g., from 220 V to 450 V).
- **Evaluating each candidate:** For each torque–speed operating point in the powertrain, compute the total losses (motor and inverter) at every candidate voltage using the comprehensive loss analysis framework.
- **Selecting the best candidate:** Pick the voltage that yields the lowest losses at each operating point.

This allocation aimed to achieve the lowest possible losses in each highlighted region, as shown in Figure 16 for both the machine and the inverter, separately. This approach effectively performs an offline optimization, generating a precomputed "optimal voltage vs. speed–torque" map that serves as a foundational reference for designing or evaluating control strategies that utilize dynamic DC-link voltage in EV powertrains.

It is important to note that, for both components, particularly in the rated speed region, a 450 V DC-link voltage was found to be the optimal value for minimizing losses. Conversely, in the low-speed region, a lower DC-link voltage of 270 V resulted in the minimum losses for both the machine and the inverter.

A closer inspection of the figures reveals that, within the inverter, a 450 V DC-bus voltage is optimal for a slightly narrower region of the rated speed compared to the machine. For example, at a speed of 4000 RPM and a torque level above 200 Nm, even a 400 V DC-link voltage can result in the minimum losses for the inverter.

C. OPTIMAL DC-LINK VOLTAGE SCHEME: COMPARING SIC VS. IGBT-BASED ELECTRIC POWERTRAIN

To verify the efficiency enhancement of SiC semiconductors compared to IGBTs, similar loss calculation methods described in Section IV-A were applied to a Si-IGBT module

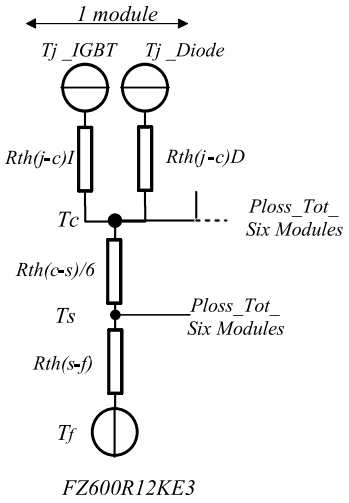

FIGURE 17. Thermal calculation model for Si-IGBT module in converter-inverter system.

with the same blocking voltage of 1200 V, FZ600R12KE3 [34], using a Si-based converter-inverter configuration shown in Figure 1 for comparison.

In calculating inverter power losses, the conduction losses for the Si-IGBT and diode in the Si-IGBT module are determined by integrating the product of the device current and its voltage drop [28], [35], resulting in the expressions

$$P_{\text{cond,IGBT}} = \frac{1}{2}\left(V_{\text{T}}\frac{I_{\text{p}}}{\pi} + R_{\text{f}}\frac{{I_{\text{p}}}^2}{4}\right) + \ldots m\cos\varphi\left(V_{\text{T}}\frac{I_{\text{p}}}{8} + \frac{1}{3\pi}R_{\text{f}}{I_{\text{p}}}^2\right) \quad (21)$$

$$P_{\text{cond,Diode}} = \frac{1}{2}\left(V_{\text{d}}\frac{I_{\text{p}}}{\pi} + R_{\text{d}}\frac{{I_{\text{p}}}^2}{4}\right) - \ldots m\cos\varphi\left(V_{\text{d}}\frac{I_{\text{p}}}{8} + \frac{1}{3\pi}R_{\text{d}}{I_{\text{p}}}^2\right) \quad (22)$$

where R_{f} is the IGBT on-state resistance and V_{T} is the IGBT voltage drop.

The analysis approach used for the SiC-based system was similarly applied to calculate switching losses and also diode conduction losses during blanking time in the Si-IGBT system. Additionally, the thermal model in Figure 17, using a calculation method similar to that of the SiC-based converters, was applied.

Finally, using the approach applied to the SiC-based drive system to determine the optimal DC-bus voltage, this method was applied to the same operating points across the drive regions under varying DC-bus voltages. Figure 18 shows system losses with and without a DC-DC converter for the second scenario (boosting from a 300 V battery terminal to 450 V DC-link voltage).

As expected, compared to the SiC-based system in Figure 14, the IGBT-based system experiences higher losses in both configurations: with a DC-DC converter at a 450 V DC-link, Figure 18 (b), and without a DC-DC converter at a 300 V DC-link, Figure 18 (a). However, Figure 18 (C),

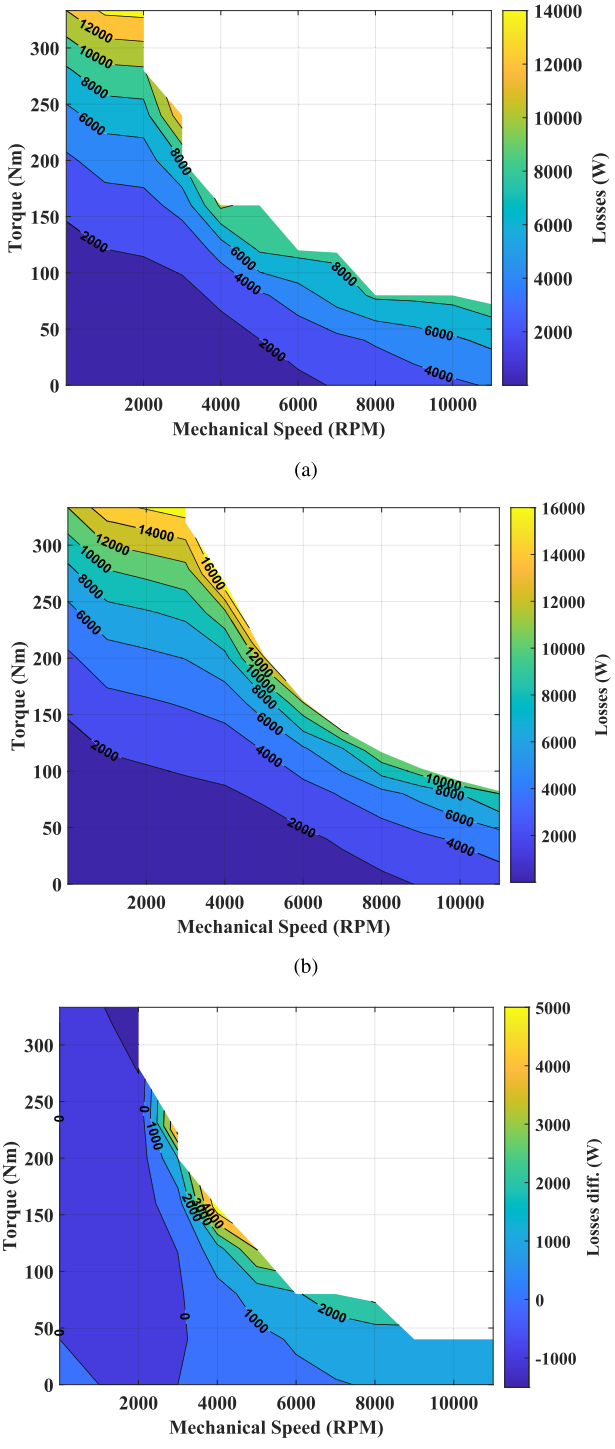

FIGURE 18. Total IGBT-based system losses and loss difference with and without DC-DC converter. (a) System losses including inverter and machine at 300V DC-bus. (b) System losses including inverter, machine, and DC-DC boost from 300V battery terminal to 450V DC bus. (c) System loss differences with and without DC-DC converter; figure(a)-figure(b).

which highlights the loss differences between configurations with and without the DC-DC converter in the IGBT system, shows a notable increase in the loss difference, in the low-speed, high-torque region marked by zero-values. This means

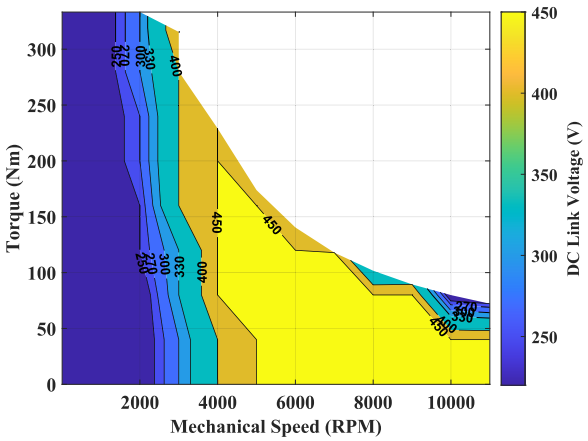

FIGURE 19. Optimum dc-bus voltages are assigned across the entire IGBT inverter operating region.

that the IGBT system operating at a 300 V DC-bus without the DC-DC converter experiences over 1 kW lower losses (as indicated on the contour bar) compared to the 450 V boosted DC-bus. This loss difference is nearly twice the one observed in the SiC system under similar conditions. However, in other drive regions, the IGBT system is almost on par with the SiC system in terms of the loss difference between including and excluding the DC-DC converter.

This can be explained by the fact that in the low-speed region, inverter switching losses are primarily influenced by the DC-link voltage—higher DC-link voltages lead to higher switching losses. Accordingly, IGBTs which have higher switching energies compared to SiC semiconductors, experience greater losses.

Consequently, by adjusting an optimal DC-link voltage for each operating point, based on the proposed optimal DC-link determination method in this study (Section IV-B), the electric powertrain system can be optimized for improved efficiency. The method which is derived from the detailed loss maps, can also be integrated as a reference map within a real-time control algorithm—such as the one outlined in the authors' previous work [19]—to optimize both IGBT- and SiC-based powertrains, leveraging dynamic DC-link voltage. Figure 19 shows the optimal DC-link voltages across the entire driveline, minimizing losses at each operating point for the IGBT inverter. As depicted, while a 450V DC-bus voltage is identified as optimal for the medium-to-high speed region in both the IGBT-based and the SiC-based inverters, it covers a slightly smaller portion of the high-speed region in the IGBT-based inverter.

D. OPTIMAL DC-LINK VOLTAGE SCHEME: DRIVE CYCLE AND ENERGY LOSS ANALYSIS, COMPARING SIC VS. IGBT-BASED ELECTRIC POWERTRAIN

In this section, the electric machine under study is incorporated into the powertrain of a medium-sized battery electric vehicle (BEV) and evaluated under the Worldwide harmonized Light vehicle Test drive Cycle (WLTC) to analyze the accumulated energy losses. WLTC is considered one of the most comprehensive drive cycles for assessing the energy efficiency of EVs, as it accurately reflects real-world driving conditions, including urban, suburban, and highway driving.

TABLE 4. Electric vehicle parameters.

Parameter	Abbreviation	Value	Unit
Aerodynamic drag coefficient	C_d	0.340	NA
Frontal area	A_f	2.300	m^2
Air density	ρ_a	1.2	kg/m^3
Rolling resistance coefficient	C_r	0.009	NA
Vehicle mass	m	1700	kg
Tire radius	r_t	0.28	m
Gear ratio	R_g	12.5	NA

Three case studies are examined. In Case A, the powertrain system operates without a DC-DC converter, using a 300 V DC-bus voltage. Case B incorporates the DC-DC converter, boosting the 300 V battery terminal voltage to a 450 V DC-link. Case C implements the proposed method in the current study, adjusting the DC-link voltage to an optimal level for the drive system. These case studies were conducted for both SiC- and IGBT-based systems.

The vehicle model parameters (e.g., mass, drag, rolling resistance), determine the torque and speed demands on the PMSM. These operating points—torque and speed values—are then used in the powertrain loss calculations, ensuring that each real-world driving scenario is accurately reflected in the final power loss assessment.

The vehicle dynamics and forces on the vehicle can be described according to [36], as

$$F_{wheel} = \frac{\rho_a}{2} C_d A_f v^2 + C_r mgcos\alpha + mgsin\alpha + m\frac{dv}{dt} \quad (23)$$

where ρ_a represents the air density, C_d is the aerodynamic drag coefficient. m is the vehicle mass, g is the gravitational constant, α is the road inclination angle, C_r is the dimensionless rolling resistance coefficient. The parameter A_f is the effective cross sectional area. The power required by the wheels to sustain a certain speed is then obtained by $P_{wheel} = F_{wheel}(t)v_{car}(t)$. The total accumulated energy consumed at the wheels is determined as,

$$E_{wheel}(t) = \int P_{wheel}(t)dt \quad (24)$$

The dynamic parameters of the vehicle are presented in Table 4 and Figure 20 illustrates the WLTC torque-speed curve for the studied SiC-based powertrain. As indicated in the dashed blue, the primary driving region occupies the low-to-mid speed range, where EVs predominantly operate. And finally Figure 21 shows the results of vehicle assessment in the WLTC drive cycle.

As shown, the SiC-based drive consistently achieves lower energy losses than the IGBT-based system across all three cases. In Cases A (300 V DC-link without DC-DC converter) and B (boosted to 450 V DC-link with DC-DC converter),

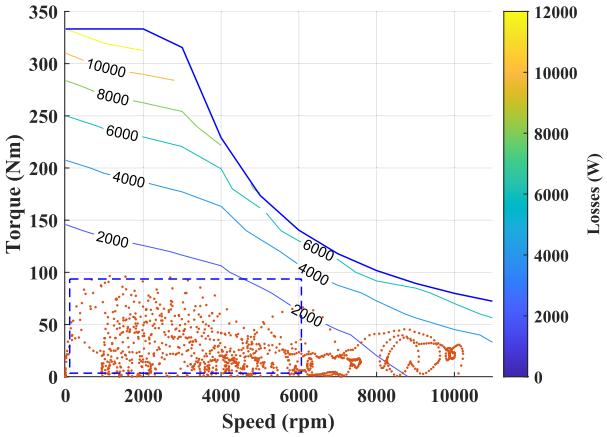

FIGURE 20. WLTC torque-speed curve for the studied SiC-based powertrain.

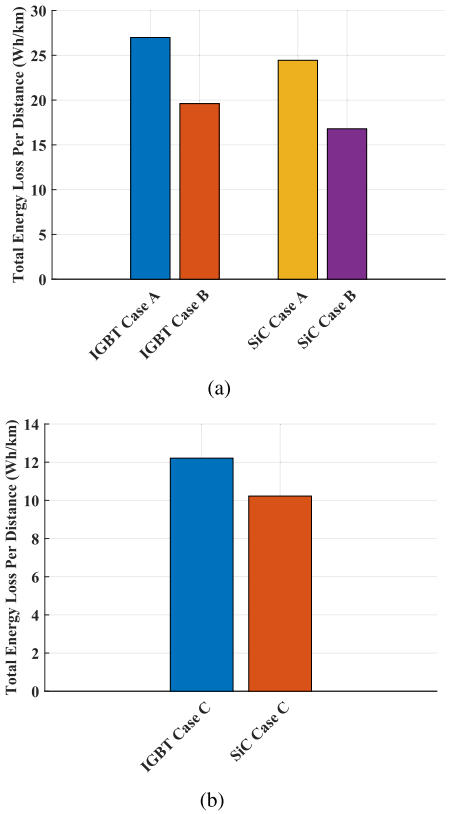

FIGURE 21. Total energy loss per distance in a selected electric vehicle in WLTC test drive cycle.(a) Case A and B for both IGBT and SiC-based systems. (b) Case C uses the optimal DC-link voltage profile for both systems.

both IGBT and SiC systems demonstrate a significant reduction in accumulated energy losses at the higher 450 V DC-link voltage, with a 27 % reduction for the IGBT system and a 31.7 % reduction for the SiC system over the WLTC drive pattern. This indicates that boosting to a higher DC-bus voltage benefits both IGBT- and SiC-based powertrains. In Case C, where the proposed adjusted DC-link voltage profile is applied across the entire driveline, the accumulated energy losses in both the IGBT and SiC systems decrease by nearly half compared to when using fixed DC-link voltages of 300 V and the boosted 450 V (Case A and B). Additionally, in Case C, the SiC-based powertrain achieves a 16 % greater energy loss reduction compared to the IGBT counterpart when optimizing the DC-link voltage across all operating regions. In general, an optimized, adjustable DC-link voltage enhances driveline efficiency in both IGBT- and SiC-based systems. However, the energy loss difference between SiC and IGBT systems is less notable with an adjustable DC-link voltage because the IGBT's losses (especially switching losses) benefit more from the reduction in voltage (whitin the adjusted DC-link voltage profile), whereas SiC MOSFETs, already are optimized for high-voltage operation, and then they experience a smaller improvement.

V. CONCLUSION

This study examined the potential for improving the efficiency of a powertrain with an adjustable DC-link voltage, integrated with a DC-DC boost converter, to determine the optimal system-level DC-link voltage across the entire torque-speed drive map. The mapping of the adjusted DC-link voltage for both SiC and IGBT-based drivetrains across the full vehicle operating range effectively reduces overall powertrain losses, particularly when low battery SoC levels are considered. However, the implementation of an optimized variable DC-link voltage strategy should be carefully evaluated.

In this work, a comprehensive system-level analysis of power losses in the electric powertrain—including FEM analysis of machine losses alongside accurate numerical evaluation of converter-inverter losses—provided a reliable method for identifying the optimal DC-link voltage across operating regions within a loss minimization framework.

Consequently, the analysis revealed that, although both IGBT- and SiC-based systems demonstrated significant reductions in accumulated energy losses at a higher fixed boosted 450 V DC-link voltage—27% for the IGBT system and 31.7% for the SiC system over the WLTC drive cycle—the proposed optimal DC-link voltage profile achieved even greater reductions. Specifically, applying the optimal DC-link voltage profile, as compared to a fixed unboosted DC-bus voltage of 300 V, reduced the energy losses by 58% for the SiC-based system and 54% for the IGBT-based drive. Additionally, reductions of over 30% were observed when compared to a fixed boosted 450 V DC-bus.

In addition, applying the optimal DC-link voltage profile resulted in up to a 16% reduction in accumulated energy loss over the WLTC driving cycle for the SiC drive system compared to the IGBT counterpart.

These findings also highlight that the benefits of an adjustable DC-link voltage, achieved through a DC-DC converter, are enhanced with the use of MOSFETs. The main contributors to this efficiency improvement are the reductions in inverter losses. Additionally, the extra power electronics losses introduced by the DC-DC converter are

almost negligible when MOSFETs are used. This minimal loss contribution further enhances the energy-saving potential of adjustable DC-link voltage powertrains.

To conclude, considering all the benefits discussed, the authors state that, generally, an adjustable DC-link voltage with a DC-DC converter may not be necessary when designing a new and unique driveline. However, situations may arise, such as reusing battery packs across different power levels within a vehicle series, developing a parallel vehicle series, or carrying over an older battery pack, where the battery voltage is not optimized for the inverter/electric machine voltage level. In these instances, incorporating an adjustable DC-link voltage with a DC-DC converter becomes crucial to ensuring efficient and optimal powertrain performance.

For future work, this study can be extended with a more detailed thermal analysis to capture the transient thermal effects. A real-time control scheme, whether closed-loop or predictive, could dynamically adjust the DC-link voltage setpoint using the proposed optimal map in this study. Additionally, while the WLTC drive cycle provides a solid foundation, evaluating additional driving cycles would expand the assessment to broader operating conditions. Incorporating the above-mentioned factors will refine the system-level loss estimations, ensuring a more precise determination of the optimal DC-link voltage for electric drive systems. However, experimental validation remains essential. While test setups may not replicate all FEM parameters and conditions, they can complement the findings, strengthening real-world applicability.

REFERENCES

[1] M. Rahimo, F. Canales, R. A. Minamisawa, C. Papadopoulos, U. Vemulapati, A. Mihaila, S. Kicin, and U. Drofenik, "Characterization of a silicon IGBT and silicon carbide MOSFET cross-switch hybrid," *IEEE Trans. Power Electron.*, vol. 30, no. 9, pp. 4638–4642, Sep. 2015.

[2] K. Kumar, M. Bertoluzzo, and G. Buja, "Impact of SiC MOSFET traction inverters on compact-class electric car range," in *Proc. IEEE Int. Conf. Power Electron., Drives Energy Syst. (PEDES)*, Dec. 2014, pp. 1–6.

[3] J. Biela, M. Schweizer, S. Waffler, and J. W. Kolar, "SiC versus Si—Evaluation of potentials for performance improvement of inverter and DC–DC converter systems by SiC power semiconductors," *IEEE Trans. Ind. Electron.*, vol. 58, no. 7, pp. 2872–2882, Jul. 2011.

[4] J.-H. Lee, C.-Y. Won, B.-K. Lee, H.-B. Kim, J.-H. Baek, K.-B. Han, and U.-I. Chung, "IPMSM torque control method considering DC-link voltage variation and friction torque for EV/HEV applications," in *Proc. IEEE Vehicle Power Propuls. Conf.*, Oct. 2012, pp. 1063–1069.

[5] J. H. Lee, J. H. Lee, J. H. Park, and C. Y. Won, "Field-weakening strategy in condition of DC-link voltage variation using on electric vehicle of IPMSM," in *Proc. Int. Conf. Electr. Mach. Syst.*, Aug. 2011, pp. 1–6.

[6] N. Zhao, N. Schofield, and W. Niu, "Energy storage system for a port crane hybrid power-train," *IEEE Trans. Transport. Electrific.*, vol. 2, no. 4, pp. 480–492, Dec. 2016.

[7] K. K. Prabhakar, M. Ramesh, A. Dalal, C. U. Reddy, A. K. Singh, and P. Kumar, "Efficiency investigation for electric vehicle powertrain with variable DC-link bus voltage," in *Proc. 42nd Annu. Conf. IEEE Ind. Electron. Soc. (IECON)*, Oct. 2016, pp. 1796–1801.

[8] N. Zhao, N. Schofield, R. Yang, and R. Gu, "Investigation of DC-link voltage and temperature variations on EV traction system design," *IEEE Trans. Ind. Appl.*, vol. 53, no. 4, pp. 3707–3718, Jul. 2017.

[9] A. Sewergin, A. H. Wienhausen, K. Oberdieck, and R. W. De Doncker, "Modular bidirectional full-SiC DC–DC converter for automotive applications," in *Proc. IEEE 12th Int. Conf. Power Electron. Drive Syst. (PEDS)*, Dec. 2017, pp. 277–281.

[10] A. Najmabadi, K. Humphries, and B. Boulet, "Implementation of a bidirectional DC–DC in electric powertrains for drive cycles used by medium duty delivery trucks," in *Proc. IEEE Energy Convers. Congr. Expo. (ECCE)*, Sep. 2015, pp. 1338–1345.

[11] J. O. Estima and A. J. Marques Cardoso, "Efficiency analysis of drive train topologies applied to electric/hybrid vehicles," *IEEE Trans. Veh. Technol.*, vol. 61, no. 3, pp. 1021–1031, Mar. 2012.

[12] S. Tenner, S. Gimther, and W. Hofmann, "Loss minimization of electric drive systems using a DC/DC converter and an optimized battery voltage in automotive applications," in *Proc. IEEE Vehicle Power Propuls. Conf.*, Sep. 2011, pp. 1–7.

[13] K. Yamamoto, K. Shinohara, and T. Nagahama, "Characteristics of permanent-magnet synchronous motor driven by PWM inverter with voltage booster," *IEEE Trans. Ind. Appl.*, vol. 40, no. 4, pp. 1145–1152, Jul. 2004.

[14] T. Schoenen, M. S. Kunter, M. D. Hennen, and R. W. De Doncker, "Advantages of a variable DC-link voltage by using a DC–DC converter in hybrid-electric vehicles," in *Proc. IEEE Vehicle Power Propuls. Conf.*, Sep. 2010, pp. 1–5.

[15] C.-Y. Yu, J. Tamura, and R. D. Lorenz, "Control method for calculating optimum DC bus voltage to improve drive system efficiency in variable DC bus drive systems," in *Proc. IEEE Energy Convers. Congr. Expo. (ECCE)*, Sep. 2012, pp. 2992–2999.

[16] C.-Y. Yu, J. Tamura, and R. D. Lorenz, "Optimum DC bus voltage analysis and calculation method for inverters/motors with variable DC bus voltage," *IEEE Trans. Ind. Appl.*, vol. 49, no. 6, pp. 2619–2627, Nov. 2013.

[17] J. Lemmens, J. Driesen, and P. Vanassche, "Dynamic DC-link voltage adaptation for thermal management of traction drives," in *Proc. IEEE Energy Convers. Congr. Expo.*, Sep. 2013, pp. 180–187.

[18] S. Sridharan and P. T. Krein, "Optimizing variable DC link voltage for an induction motor drive under dynamic conditions," in *Proc. IEEE Transp. Electrific. Conf. Expo (ITEC)*, Jun. 2015, pp. 1–6.

[19] Y. Xu, A. Kersten, S. Klacar, and D. Sedarsky, "Maximizing efficiency in smart adjustable DC link powertrains with IGBTs and SiC MOSFETs via optimized DC-link voltage control," *Batteries*, vol. 9, no. 6, p. 302, May 2023.

[20] S. Amirpour, T. Thiringer, and Y. Xu, "Mapping an optimum DC-link voltage across the entire SiC-based EV drive regions using a synchronous boost DC–DC converter," SAE Tech. Paper, Tech. Rep. 2024-01-2218, 2024.

[21] M. Meyer and J. Bocker, "Optimum control for interior permanent magnet synchronous motors (IPMSM) in constant torque and flux weakening range," in *Proc. 12th Int. Power Electron. Motion Control Conf.*, Aug. 2006, pp. 282–286.

[22] M. Meyer, T. Grote, and J. Böcker, "Direct torque control for interior permanent magnet synchronous motors with respect to optimal efficiency," in *Proc. Eur. Conf. Power Electron. Appl.*, Jan. 2007, pp. 1–9.

[23] *CAB450M12XM3*. Wolfspeed. Accessed: Feb. 27, 2025. [Online]. Available: https://assets.wolfspeed.com/uploads/2024/01/Wolfspeed_CAB450M12XM3_data_sheet.pdf

[24] S. Amirpour, T. Thiringer, and D. Hagstedt, "Power loss analysis in a SiC/IGBT propulsion inverter including blanking time, MOSFET's reverse conduction and the effect of thermal feedback using a PMSM model," in *Proc. IECON 46th Annu. Conf. IEEE Ind. Electron. Soc.*, Oct. 2020, pp. 1424–1430.

[25] A. Acquaviva and T. Thiringer, "Energy efficiency of a SiC MOSFET propulsion inverter accounting for the MOSFET's reverse conduction and the blanking time," in *Proc. 19th Eur. Conf. Power Electron. Appl. (EPE ECCE Eur.)*, Sep. 2017, pp. P.1–P.9.

[26] J. W. Kolar, H. Ertl, and F. C. Zach, "Influence of the modulation method on the conduction and switching losses of a PWM converter system," in *Proc. Conf. Rec. IEEE Ind. Appl. Soc. Annu. Meeting*, Seattle, WA, USA, Nov. 1990, pp. 502–512.

[27] S. Amirpour, T. Thiringer, and D. Hagstedt, "Energy loss analysis in a SiC/IGBT propulsion inverter over drive cycles considering blanking time, MOSFET's reverse conduction and the effect of thermal feedback," in *Proc. IEEE Energy Convers. Congr. Expo. (ECCE)*, Oct. 2020, pp. 1505–1511.

[28] *Application Manual Power Semiconductors*, SEMIKRON, Ilmenau, Germany, 2015, pp. 274–279.
[29] *Application Note Thermal Resistances of IGBT Modules–specification and Modelling*, SEMIKRON, Nuremberg, Germany, 2014.
[30] *Wieland Microcool CP3012*. Accessed: Feb. 27, 2025. [Online]. Available: https://www.microcooling.com/wp-content/uploads/2019/08/CP3012_datasheet.pdf
[31] *MAGNETICS. 0078163A7*. Accessed: Feb. 27, 2025. [Online]. Available: https://www.mag-inc.com/Media/Magnetics/Datasheets/0078163A7.pdf
[32] Magn. (2024). *2024 MAGNETICS Powder Cores Catalog*. [Online]. Available: https://www.mag-Inc.com/Company/News/January-2024/New-2024-Powder-Cores-Catalog
[33] S. Ehrlich, C. Joffe, H. Thielke, M. Leinfelder, and M. März, "Comprehensive SPICE model for power inductor losses," in *Proc. IEEE Appl. Power Electron. Conf. Expo. (APEC)*, Mar. 2019, pp. 1237–1244.
[34] *Infineon. FZ600R12KE3*. Accessed: Feb. 27, 2024. [Online]. Available: https://www.infineon.com/cms/en/product/power/igbt/igbt-modules/fz600r12ke3/
[35] F. Casanellas, "Losses in PWM inverters using IGBTs," *IEE Proc.-Electr. Power Appl.*, vol. 141, no. 5, pp. 235–239, 1994.
[36] E. Grunditz, "BEV powertrain component sizing with respect to performance, energy consumption and driving patterns," M.S. thesis, Dept. of Energy and Environment, Chalmers Univ. Technol., Gothenburg, Sweden, 2014.

SEPIDEH AMIRPOUR received the B.Sc. degree in electrical engineering from the University of Guilan, Rasht, Iran, in 2004, and the M.Sc. degree in electrical engineering from Kempten University of Applied Sciences, Germany, in 2013. She is currently pursuing the Industrial Ph.D. degree with the Chalmers University of Technology in a joint program with ZEEKR.

Since 2016, she has been an Electric Drive Specialist with the Department of Vehicle Electronics and Software, ZEEKR Technology Europe, Gothenburg, Sweden. Her area of interest is power electronics in automotive and telecommunication applications. Her current research interests include SiC/Si-based converter applications, electrical machines, and motor drive topologies focusing on power and energy loss modeling and optimization, thermal modeling, and reliability in the electric/hybrid powertrain.

TORBJÖRN THIRINGER (Senior Member, IEEE) received the M.Sc. and Ph.D. degrees from the Chalmers University of Technology, in 1989 and 1996, respectively. He is currently a Professor of applied power electronics with the Chalmers University of Technology. His research interests include the modeling, control, and grid integration of wind energy converters into power grids and power electronics and drives e.g., for electrified vehicles, buildings, and industrial applications.

SIMA SOLTANIPOUR (Member, IEEE) received the B.Sc. degree from Arak University, Iran, in 2014, and the M.Sc. (Eng.) degree from the Chalmers University of Technology, Sweden, in 2020, where she is currently pursuing the Ph.D. degree in a joint program with Volvo Cars Corporation, Gothenburg, Sweden. She joined Volvo Cars Corporation, as an Industrial Ph.D. Student, in 2021.

YU XU (Member, IEEE) received the dual B.Sc. degree in vehicle engineering and mechanical engineering from Beijing Institute of Technology and Politecnico di Torino, in 2018, and the M.Sc. degree in vehicle engineering from the KTH Royal Institute of Technology, in 2020. He is currently pursuing the Industrial Ph.D. degree with the Chalmers University of Technology through a joint program with ZEEKR. Since then, he has been a CAE Engineer with the Department of Powertrain Engineering, ZEEKR Technology Europe, Gothenburg, Sweden. His research interest includes developing energy-efficient powertrains for pure electric vehicles.